Journal of Materials Chemistry C

Accepted Manuscript

This article can be cited before page numbers have been issued, to do this please use: T. Frömling, S. Steiner, A. Ayrikyan, D. Bremecker, M. Duerrschnabel, L. Molina, H. Kleebe, H. Hutter, K. G. Webber and M. Acosta, *J. Mater. Chem. C*, 2017, DOI: 10.1039/C7TC03975A.

View Article Online
DOI: 10.1039/C7TC03975A

Journal of Materials Chemistry C

ARTICLE

Received 00th January 20xx,
Accepted 00th January 20xx

DOI: 10.1039/x0xx00000x

www.rsc.org/

Designing Properties of $(Na_{1/2}Bi_x)TiO_3$-Based Materials Through *A*-Site Non-Stoichiometry

Till Frömling[a], Sebastian Steiner[a], Azatuhi Ayrikyan[b], Daniel Bremecker[a], Michael Dürrschnabel[a], Leopoldo Molina-Luna[a], Hans-Joachim Kleebe[a], Herbert Hutter[c], Kyle G. Webber[b], Matias Acosta[d]

Point defects largely determine the properties of functional oxides. So far, limited knowledge exists on the impact of cation vacancies on electroceramics, especially in $(Na_{1/2}Bi_{1/2})TiO_3$ (NBT)-based materials. Here, we report on the drastic effect of *A*-site non-stoichiometry on the cation diffusion and functional properties in the representative ferroelectric $(Na_{1/2}Bi_{1/2})TiO_3$-$SrTiO_3$ (NBT-ST). Experiments on NBT/ST bilayers and NBT-ST with Bi non-stoichiometry reveal that Sr^{2+}-diffusion is enhanced by up to six orders of magnitude along the grain boundaries in Bi-deficient material as compared to Bi-excess material with values of grain boundary diffusion ~10^{-8} cm^2/s and ~ 10^{-13} cm^2/s in the bulk. This also means a nine orders of magnitude higher diffusion coefficient compared to reports from other Sr-diffusion coefficients in ceramics. Bi-excess leads to the formation of a material with a core-shell microstructure. This results in 38% higher strain and one order of magnitude lower remanent polarization. In contrast, Bi-deficiency leads to a ceramic with a grain size six times larger than in the Bi-excess material and homogeneous distribution of compounds. Thus, the work sheds light on the rich opportunities that *A*-site stoichiometry offers to tailor NBT-based materials microstructure, transport properties, and electromechanical properties.

Introduction

Ceramics based on $(Na_{1/2}Bi_{1/2})TiO_3$ (NBT) are strong lead-free candidates to substitute hazardous lead-based piezoelectric materials.[1] Considerable progress has been made in the development of these materials, which under certain conditions display even better properties than lead containing materials.[2-7] Moreover, recent works demonstrated that ionic conductivity in NBT-based materials can be enhanced by several orders of magnitude by controlling their B-site defect chemistry. Despite the promising advancements, there is still a significant lack of knowledge considering the defect chemistry of NBT and its implications on microstructure, transport properties, and electromechanical properties.

Initially, it was expected that changes in defect chemistry have similar effects on NBT as on $Pb(Zr,Ti)O_3$ (PZT), which is not the case.[8, 9] Acceptor doped NBT does not display properties expected from a "hard" ferroelectric material but rather becomes an excellent oxygen ion conductor with conductivity values comparable to oxygen membrane materials such as yttria stabilized zirconia (10^{-2} S/cm at 600°C).[8, 10] The same could also be observed in *A*-site non-stoichiometric NBT, in which a Bi-deficiency led to the creation of highly mobile oxygen vacancies.[8, 9] Thus, extreme variation in NBT properties can be expected with only minor changes to the defect chemistry. A certain amount Bi-deficiency is actually expected to occur during sintering of NBT-materials due to Bi_2O_3 volatility at elevated temperatures.[11] Hence, knowledge about the changes in defect chemistry of Bi-based materials is mandatory for a rational synthesis and engineering of functional properties, including conductivity, piezoelectricity, among many others.[12]

Recently, it has been reported that chemical inhomogeneity can result in beneficial electrical properties, *e.g.*, in $(Na_{1/2}Bi_{1/2})TiO_3$-$SrTiO_3$ (NBT-ST).[13-15] A core-shell microstructure favored the development of a reversible high electrostrain at reduced electric field.[16] Despite the amount of work performed on the core-shell microstructure, other works on NBT-ST or related materials presented no evidence of a core-shell structure,[17-33] or it was proposed that no core-shell structure forms.[34, 35] The electrical properties of the NBT-ST compounds also differ, despite similar synthesis parameters.[14] This demonstrates that there is key knowledge missing in the literature, which affects the experimental reproducibility. It, in fact, seems to have implications on both the microstructure and functional properties of NBT-based materials.

In this work, NBT-ST is used as a model material for NBT-based compounds to elucidate the effect of *A*-site non-stoichiometry on microstructure and functional properties. The investigation involves interdiffusion experiments of bilayers composed of stoichiometric

[a] Department of Materials and Earth Science, Technische Universität Darmstadt, Alarich-Weiss-Strasse 2, D-64287 Darmstadt, Germany
[b] Department of Materials Science and Engineering, Friedrich-Alexander-Universität Erlangen-Nürnberg, Martensstraße 5, 91058 Erlangen, Germany
[c] Institute of Chemical Technologies and Analytics, Getreidemarkt 9/164 AC, 1060 Vienna,Austria
[d] Department of Materials Science and Metallurgy, University of Cambridge, Charles Babbage Road 27, CB3 0FS Cambridge, UK

Electronic Supplementary Information (ESI) available: ToF-SIMS images of cross sections from bilayer interdiffusion experiments sintered for 2 h, 5 h and 10 h. *Concentration of Sr^{2+} in NBT from EDX measurements after NBT/ST bilayer interdiffusion experiments sintered for a) 2 h, b) 5 h, c) 10 h and d) 10 h with Bi-excess*. See DOI: 10.1039/x0xx00000x

View Article Online
DOI: 10.1039/C7TC03975A

and non-stoichiometric NBT with ST to elucidate diffusion processes. Additionally, the impact of *A*-site non-stoichiometry on the microstructure and functional properties of bulk NBT-ST materials is also investigated.

Methods

For bilayer interdiffusion experiments NBT, NBT with a 0.1% Bi_2O_3-excess (denoted $NB_{0.501}T$), and ST powders were prepared by a conventional solid solid-state calcination method. Powdered Bi_2O_3, Na_2CO_3, and TiO_2 or $SrCO_3$ and TiO_2 (>99%, Alfa Aesar GmbH, Karlsruhe, Germany) were mixed for 24 h with zirconia balls and ethanol using a planetary ball mill (Fritsch Pulverisette 5, Idar-Oberstein, Germany). After drying, the powder mixture was calcined at 1100 °C for 5 h. The calcined powder was re-milled for 24 h. The NBT and the ST powders were pressed into discs with a uniaxial pressure of 127 MPa and pressed isostatically at 300 MPa. After that, the two green bodies were sintered together at 1150 °C for 2 h, 5 h, or 10 h. Scanning electron microscopy (SEM) investigations and subsequent grain size analysis was done on samples ground and polished down to 600 µm. Mean grain size was obtained by the mean intercept method, with a numerical multiplication factor of 1.56. Around 200 grains in different positions of the samples were measured to obtain reliable statistical information.

Bulk pellets of $0.75(Na_{1/2}Bi_x)TiO_3$-$0.25SrTiO_3$ (NB_xT-ST) ceramics with compositional range of $0.49 < x < 0.51$ were prepared by the same conventional solid state method as mentioned above. In this case the grain bodies were sintered solely for 10 h.

The structural properties of the specimens were investigated by X-ray diffraction (XRD) (AXS D8; Bruker Corporation, Karlsruhe, Germany) and scanning electron microscopy (SEM) (Philips XL30FEG; Philips, Amsterdam, Netherlands). After coating the samples with carbon by sputtering deposition, energy dispersive X-ray spectroscopy (EDX) (X-MAX; Oxford Instrument, Abingdon, UK) was conducted and back-scatter images (BSE) were recorded with a (JEOL JSM 7600F SEM operated at 15 kV; Tokyo, Japan), Additionally, time-of-flight secondary mass spectrometry (ToF-SIMS) was conducted to investigate the cation interdiffusion profiles (ToF-SIMS[5], ION-TOF, Münster, Germany). For electrical measurements, Pt electrodes were sputtered on the both surfaces of the disc shaped samples after grinding. The large signal properties such as polarization loops and strain curves were measured with the aixPSE system (aixACCT system GmbH, Aachen, Germany) at 0.5 Hz. The permittivity and the dielectric loss were measured with a HP 4284A (Hewlett Packard Corporation, Palo Alto, USA) at 1 kHz, 10 kHz, 100 kHz and 1MHZ.

Results and Discussion

Interdiffusion experiments

Bilayers of initially stoichiometric NBT and ST were synthesized for interdiffusion experiments. Additionally, a bilayer containing $NB_{0.501}T$ was prepared. At this point it is worth stressing that Bi_2O_3 volatilization during sintering has already been proven.[8, 11] Thus, the initially stoichiometric NBT is expected to become Bi-deficient in the sintering procedure, whereas the $NB_{0.501}T$ with Bi-excess is expected to become stoichiometric. The comparison of the experimental results between bilayers and bulk materials indeed confirm this working hypothesis, as it will become apparent.

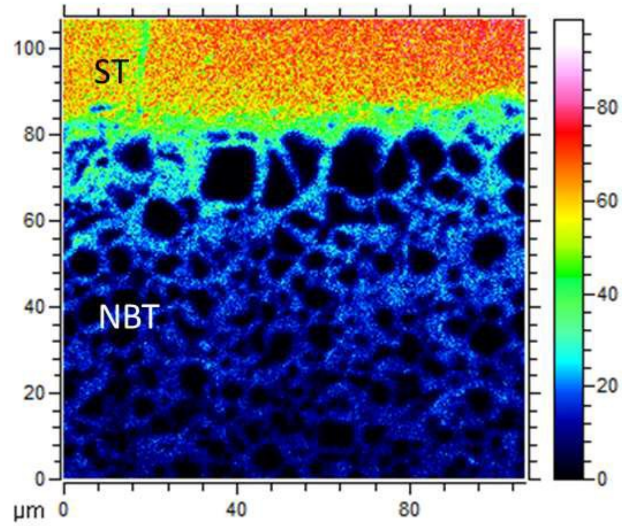

Fig. 1: SIMS image of the Sr-intensity at the cross section from the interface of ST and NBT sintered for 10 h

During sintering of the NBT/ST bilayers, interdiffusion of the components occurs across the interface, which allows for quantification of the diffusion behavior of cations during sintering. The cross sections of the respective bilayers were first investigated by ToF-SIMS. Fig. 1 depicts the Sr-signal intensity at the NBT/ST interface after sintering for 10 h. The color scale bar on the right illustrates increasing concentration from top to bottom. Hence, extended penetration of Sr^{2+} into the NBT layer is obtained during sintering. However, the Sr^{2+} is transported along pathways resembling the grain microstructure.

ToF-SIMS has a lateral resolution of approximately 100 nm and is, therefore, a useful technique to evaluate qualitatively the inhomogeneous distribution of chemical elements.[36-39] However, quantification of chemical heterogeneity is quite challenging. Thus, SEM with subsequent EDX measurements were conducted in the bilayers to obtain atomic ratios and, hence, semi-quantify existing chemical heterogeneity. In Fig. 2a) a BSE image of the interface of NBT/ST is shown. A different phase contrast is visible at the grain boundary, which is in agreement with the higher Sr^{2+}-content observed from the EDX Sr-signal of the same region in Fig. 2b). These findings and the SIMS results indicate that Sr^{2+} diffuses preferentially along the grain boundary with subsequent bulk diffusion from the boundary. The quantification of the cation content was done by summing the signal intensities along the x-axis (illustrated in Fig. 2b)) and taking into account the molar fractions of the cations. The data is plotted along the y-axis in Fig. 2c). Despite the experimental error that characterizes EDX, it is evident that Sr^{2+} transport extends further into the NBT layer than the measured range of 85 µm. There is a bulk dominated transport in Region II in Fig. 2c) from 40 at. % to 10 at. % Sr^{2+} content and a grain boundary transport in region III, starting at approximately 10 at. % Sr^{2+} content. Additionally, the Bi^{3+} and Na^{+} concentration in the ST layer (Region I) is high as well. Initially, it seems likely that this is the result of an ambipolar diffusion process.[40] If a charged Sr^{2+} is transported into the NBT, an equally charged entity or entities need to be transported in the other direction to maintain charge neutrality. However, this is most likely not the only reason for an elevated Bi^{3+} and Na^{+}-concentration on the ST side.

View Article Online
DOI: 10.1039/C7TC03975A

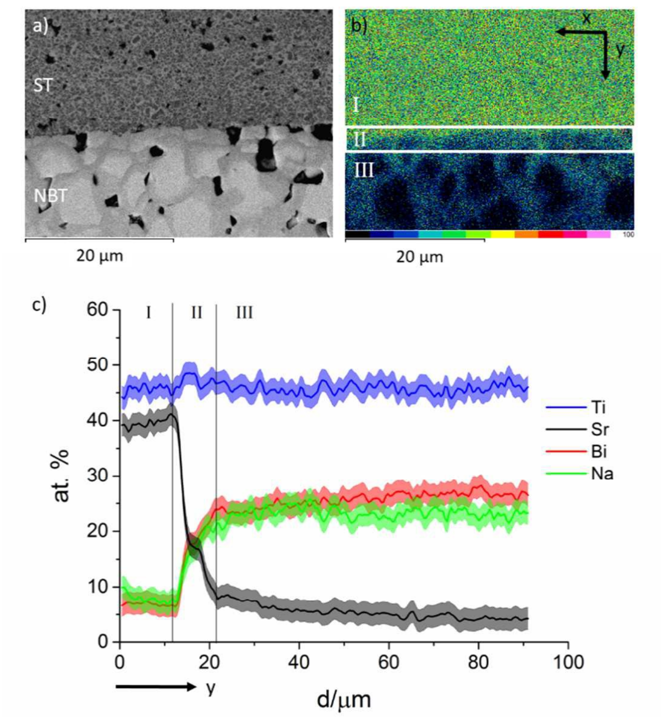

Fig. 2: a) SEM image of ST and NBT interface sintered for 10 h. b) Corresponding Sr concentration image from EDX. c) Relative concentration in at. % from the composition at the ST/NBT interface with error depicted as shaded region (sintered for 10 h).

NBT formation starts at 410 °C, whereas the formation of ST occurs at 610 °C.[14] Thus, we expect that Bi^{3+} and Na^{+} diffusion is activated at much lower temperature, leading to a much earlier formation and densification of NBT than ST. Therefore, NBT is transported into the ST side through the porous undensified grain network. Due to the stability of $SrCO_3$, we expect that Sr^{2+} becomes mobile at higher temperatures than Na and Bi.[14] Hence, the ambipolar diffusion process sets in with Sr^{2+} penetrating the densified NBT via the grain boundaries. However, the content of Sr^{2+} with respect to the cations at the beginning of the diffusion process is 40 at. % (10 at. % lower than expected) because of the NBT diffusion through the porous network prior to Sr^{2+}-diffusion. In the case of a regular NBT-ST solid-state synthesis, there would not be separated NBT and ST grains as an initial state prior to the interdiffusion. There are rather NBT grains forming with subsequent Sr^{2+}-penetration from decomposing $SrCO_3$.[14] Hence, we further investigate the Sr^{2+} diffusion into the NBT side of the NBT/ST bilayers.

The chemical or ambipolar diffusion coefficient $\widetilde{D}$ can be described by taking only the *A*-site cations into account and attributing an effective diffusion coefficient $D_{Na/Bi}$ to the transport of Na^{+} and Bi^{3+}:[40]

$$\widetilde{D} = \frac{D_{Sr} \cdot D_{Na/Bi}}{D_{Sr} + D_{Na/Bi}} \approx D_{Sr} \, , \tag{1}$$

where D_{Sr} represents the diffusion coefficient for Sr^{2+}. We assume that $D_{Na/Bi} \gg D_{Sr}$ because of the earlier formation of NBT than ST. Therefore, our estimation relies on a higher mobility of Na^{+} and Bi^{3+}. Thus, the ambipolar diffusion coefficient (in bulk and grain boundary) should be almost solely dependent on D_{Sr}. It is therefore sufficient to determine the Sr^{2+} diffusion coefficient from Fig. 2c) to evaluate the ambipolar diffusion. The approach by Whipple and LeClaire was used to describe the bulk diffusion process with additional grain boundary diffusion.[41, 42] For this, the natural logarithm of the concentration or fraction c is plotted against the distance d to the power of 6/5 (see supplementary information). This leads to a linear plot in the grain boundary diffusion region (region III in Fig. 2c)). The grain boundary diffusion coefficient D_{gb} can be obtained from the slope according to:

$$s \cdot D_{gb} \cdot \delta = 1.322 \cdot \left(\frac{D_b}{t}\right)^{1/2} \cdot \left(\frac{\partial \ln c}{\partial d^{6/5}}\right)^{-5/3} , \tag{2}$$

where $\boldsymbol{D_b}$ the bulk diffusion coefficient, $\boldsymbol{t}$ the diffusion time, $\boldsymbol{\delta}$ the grain boundary thickness, and $\boldsymbol{s}$ the segregation coefficient. While the grain boundary thickness can be estimated to be in the nm regime, the segregation coefficient is more difficult to determine.[37] Hence, the value $\boldsymbol{s \cdot D_{gb}}$ is further discussed. The bulk diffusion coefficient can be calculated from the steep decent of the profile close to the interface (region II), which is dominated by the impact of bulk diffusion. Thus, it can be fitted by a regular error function approach.[43] The results from diffusion experiments lasting 2 h, 5 h, and 10 h are given in Table 1.

Table 1: Diffusion coefficients of Sr^{2+} in NBT at 1050°C (assuming $\delta = 1$ nm).

	$\boldsymbol{D_b}$/(cm²/s)	$\boldsymbol{s \cdot D_{gb}}$/(cm²/s)
10 h	$2.0 \cdot 10^{-13}$	$3.4 \cdot 10^{-8}$
5 h	$5.7 \cdot 10^{-13}$	$9.5 \cdot 10^{-8}$
2 h	$2.9 \cdot 10^{-13}$	$6.8 \cdot 10^{-8}$

The values obtained for bulk or grain boundary diffusion coefficients of the two experiments are very similar and in acceptable agreement. The values themselves are extremely high in comparison to diffusion coefficients of Sr^{2+} in barium titanate or gadolinium doped ceria, for example, which were in the range of

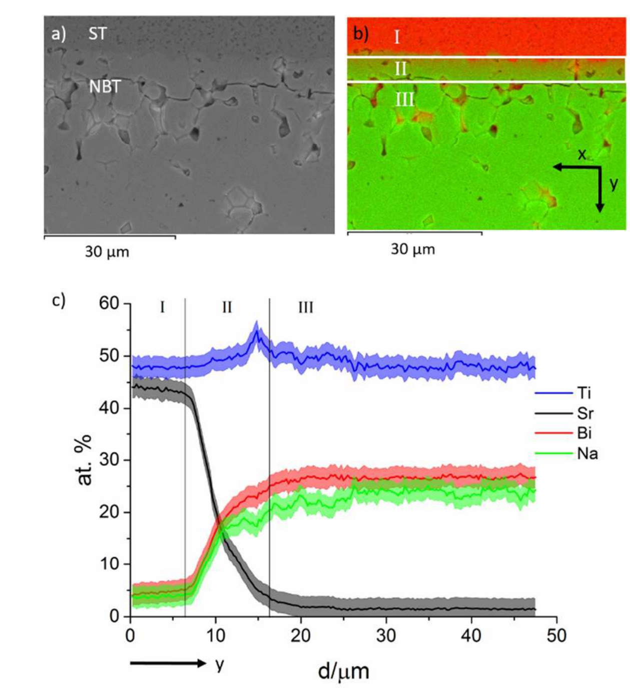

Fig. 3: a) SEM image of ST/$NB_{0.501}T$ interface of an interdiffusion experiment at 1050°C for 10h. b) Corresponding overlay image of Sr(red) and Bi(green) concentration. c) Relative concentration in at. % from the composition at the ST/ $NB_{0.501}T$ with error depicted as shaded region (sintered for 10 h).

View Article Online
DOI: 10.1039/C7TC03975A

10^{-17} cm^2/s at the same temperature.[44, 45] Grain boundary diffusion coefficients are even a further five orders of magnitude larger (assuming a small impact of the segregation factor). Therefore, the diffusion coefficients of Sr^{2+} in NBT-ST are four orders of magnitude higher in the bulk and nine orders of magnitude higher along grain boundaries than the previously reported Sr^{2+} diffusion coefficients in ceramics.[44, 45] Thus, extraordinarily fast transport of Sr^{2+} occurs along grain boundaries in the NBT/ST bilayers.

The most likely ambipolar diffusion mechanism, rendering this fast Sr^{2+}-migration along grain boundaries, is a vacancy mechanism on the *A*-site. Both a low activation energy for cation transport and a high concentration of vacancies can increase the diffusion rate. It is known that NBT becomes highly (oxygen) ionically conductive when Bi_2O_3 evaporates during the sintering process and leaves an increased concentration of oxygen vacancies.[9, 11] Therefore, our hypothesis is that the corresponding Bi-vacancies are also mobile and facilitate the ambipolar diffusion. To test this, a bilayer with excess of Bi (0.1 mol %) in the NBT layer ($NB_{0.501}T$) was used for further analysis in order to compensate the evaporation of Bi during sintering.

The SEM image and the EDX overlay image of Sr- and Bi-signals is given in Fig. 3a) and b) for the experiment with $NB_{0.501}T$. It is evident that the penetration depth of Sr^{2+} into the $NB_{0.501}T$ layer was significantly reduced to less than 20 µm. In fact, within the error of the EDX measurement it can be expected that no Sr^{2+} diffused through the grain boundary. This is an astonishing result and further proof of a vacancy-controlled diffusion mechanism. The small excess of Bi leads to a decrease in *A*-site vacancy concentration, which is sufficient to inhibit the extensive Sr^{2+} grain boundary diffusion. Additionally, it provides significant evidence that the densification of NBT prior to Sr^{2+}-mobility is a valid assumption. In case diffusion in a porous network occurred, we would expect that Sr^{2+}-content increases along the grain boundaries for small Bi-excess as well.

Fig. 3c) depicts the cation concentration at the interface of the $NB_{0.501}T$. The first thing to notice is that transport of Bi^{3+}, Na^{+}, and Sr^{2+} is still evident. However, the Sr^{2+} does not penetrate further than 20 µm into Region III. This indicates that the Sr^{2+} diffused at least 100 µm less than in the experiment performed under same sintering conditions for NBT. The logarithmic plots of $NB_{0.501}T$ and Bi-deficient NBT also offer a good illustration of the different diffusion behavior (see supplementary information). The bulk diffusion coefficient in $NB_{0.501}T$ is also reduced compared to the Bi-deficient material. However, with a value of $1 \cdot 10^{-13}$ cm^2/s it is only reduced by a factor of 2 to 6. Nevertheless, the results presented so far demonstrate the sensitivity of cation mobility in NBT upon changes in the *A*-site stoichiometry. This has not been previously demonstrated, as earlier investigations principally focused on the possibility to tune oxygen ionic conductivity.[8, 9, 11] It is also important to note that this is most likely

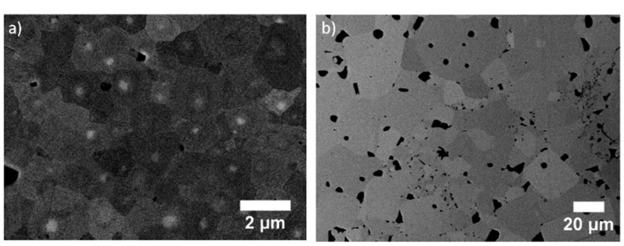

Fig. 4: SEM BSE images from a) $NB_{0.51}T$ sintered for 10 h and b) $NB_{0.49}T$ sintered for 10 h

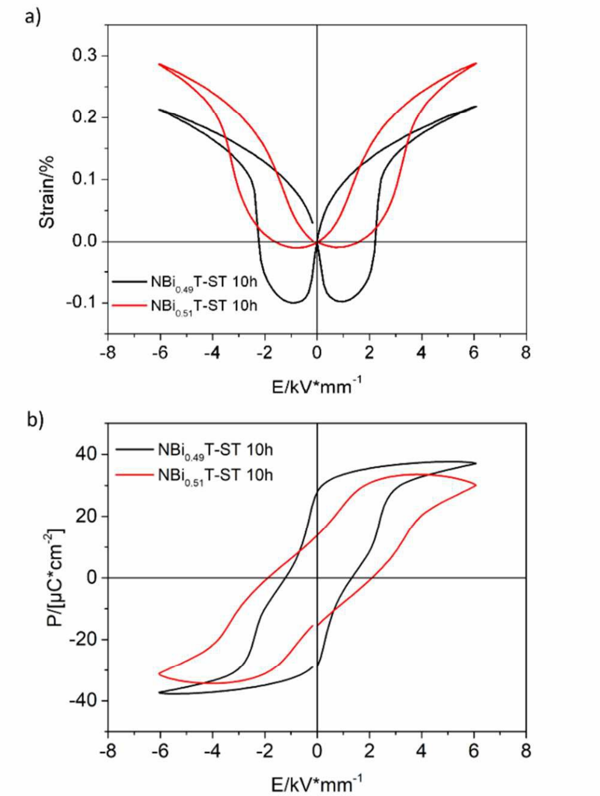

Fig. 5: Electric field dependent a) strain and b) polarization of $NB_{0.51}T$-ST and $NB_{0.49}T$-ST

the reason why some investigations reported a core-shell microstructure for NBT-ST,[13, 14] whereas others observed an apparent homogeneous solid solution.[34, 35]

Solid state synthesis of NBT-BT with different *A*-site stoichiometry

The observations are, of course, troubling and promising at the same time. On one hand, the synthesis procedure must be checked and strictly adhered to limit variations in material properties in order to obtain reproducible results. On the other hand, it also provides a clear strategy to tune NBT-based perovskite materials, as well as other functional ceramics. From the results of this work, it becomes evident that we should be able to extensively tune the microstructure of NBT-ST and, thus, the electromechanical properties through minor adjustments to the *A*-site Bi-stoichiometry.

To demonstrate the concept, we synthesized samples with a 1 mol% excess $NB_{0.51}T$-ST and a 1 mol% deficiency $NB_{0.49}T$-ST. Fig. 4 shows the microstructure of the two compositions sintered at 1150°C for 10 h. The average grain size of the Bi-excess composition is 1.4 µm. BSE SEM clearly indicates the presence of a core-shell structure, as previously reported.[13, 14] Therefore, homogenization of the material was not possible even after 10 h of sintering. $NB_{0.49}T$-ST has a grain diameter of 7.8 µm, which is almost 6 times larger than for $NB_{0.51}T$-ST. It is important to note that oxygen vacancy concentration plays a considerable role in grain growth. Recently, it has been proposed that roughening or faceting of the grain boundary structure depending on the oxygen vacancy concentration leads to a change in grain size.[46-48]

View Article Online
DOI: 10.1039/C7TC03975A

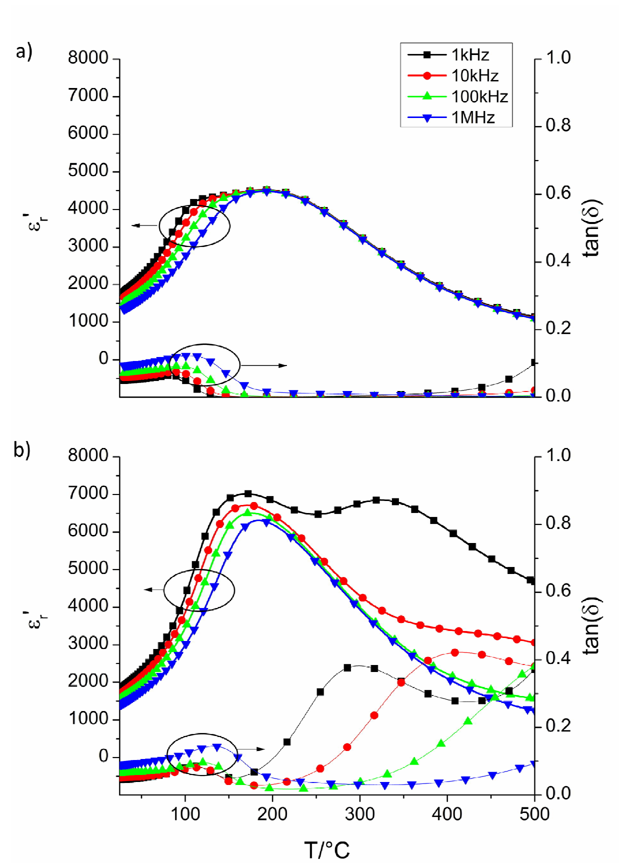

Fig. 6: Real part of permittivity ε'_r and dielectric loss tan(δ) for a) $NB_{0.51}$T-BT and b) $NB_{0.49}$T-BT at different frequencies.

The enhanced *A*-site vacancy-controlled diffusion in $NB_{0.49}$T-ST leads to a good homogeneity and grain growth of the sample as consequence of the complete Sr^{2+} diffusion through the grains. This renders that, within the detection limit of our SEM, it was not possible to observe a core-shell microstructure in $NB_{0.49}$T-ST. $NB_{0.51}$T-ST has the expected high field response for a core-shell relaxor ferroelectric with very high strains of up to 0.3% and reduced remanent polarization.[13, 14] $NB_{0.49}$T-ST, however, shows a rather ferroelectric like field-strain relationship (Fig. 5a)). Tuning the microstructure with a core-shell, in fact, resulted in a 38% enhancement in the unipolar strain. Due to pinching in the polarization hysteresis loop of $NB_{0.49}$T-ST, the remanent polarization of 27.84 μC/cm^2 is 100% larger than in $NB_{0.51}$T-ST. The loop still presents pinching, as depicted in Fig. 5b). This may suggest that the persistence of chemical inhomogeneity on a local scale (different A-site and B-site cations) lead to a destabilization of the ferroelectric state. Given the polarization and strain loop features in both materials, we do expect that they both present the archetypal response of a field induced phase transition.[49-53] Undoubtedly, the presence of oxygen vacancies and concomitant pinning of ferroelectric domains could also influence this transition when comparing both materials. A detail description of the relationship between oxygen vacancies and the field induced phase transition is, however, out of the scope of the present work.

From the temperature dependent permittivity ε'_r and dielectric loss tan(δ) in Fig. 6, it can be seen that the dielectric properties are significantly affected. The core-shell material $NB_{0.51}$T-ST (Fig. 6a)) shows a response often presented for NBT and some of its solid solutions.[54] $NB_{0.49}$T-ST, however, has two very distinctive dielectric responses with the second one at high temperatures being highly frequency dependent (Fig. 6 b)). This is often attributed to the presence of short range movement of oxygen vacancies or the change in properties of high temperature polar nano regions, as discussed for NBT-BT.[55-59] An in depth discussion is, however, left for future work. The herewith presented results show that actual NBT-ST properties still need to be properly determined to fully assess the impact of point defects and core shell structures on the electrical properties of the material.

The results highlight the importance of these areas of research for other NBT-based piezoelectrics. For example, *A*-site vacancies are also most likely the cause for the different properties found for NBT-BT with different *A*-site vacancy concentrations[46] and Zr-doped NBT-BT core-shell development in some works, but not in all.[60, 61] Comparing the results for *A*-site non-stoichiometric NBT-BT with NBT-ST, the oxygen vacancies induced by Bi-deficiency are not as mobile as in pure NBT. Hence, the material is still highly resistive at room temperature and can be subjected to high electric fields (Fig. 5).[46] There is also a similar trend in grain size for NBT-BT and NBT-ST. Moreover, the ferroelectric properties are also modified to a great extent depending on the Bi-content. This clearly shows the potential of microstructure (*i.e.*, core-shell and grain size) and property control that tuning *A*-site vacancies may offer in NBT related materials.

Conclusions

The microstructure and properties of NBT-ST can be controlled to a great extent by the *A*-site non-stoichiometry. Experiments in NBT/ST bilayers showed that the incorporation of Sr^{2+} into the NBT-lattice occurs via vacancy mediated transport. The higher vacancy concentration results in a dramatic enhancement of up to six orders of magnitude in Sr^{2+} transport along grain boundaries. Namely, the calculated diffusion coefficients for bulk is on the order of 10^{-13} cm^2/s, whereas at grain boundary on the order of 10^{-8} cm^2/s. The core-shell microstructure of bulk NBT-ST samples is a result of a very low concentration of Bi-vacancies. Bi-deficient NBT-ST, in contrast, features no core-shell microstructure and six times larger grain size. By tuning the core-shell microstructure through controlling the *A*-site non-stoichiometry of NBT-ST, we enhanced the strain response by 38 % and reduced the remanent polarization by an order of magnitude. This work helps explains the large variations in microstructure and electrical properties of previously published data on NBT-based materials and emphasizes the importance of further defect chemistry investigations. The results of this work highlight the substantial microstructural and property effects that *A*-site defect chemistry can have. A simple control of the *A*-site stoichiometric can thus be used as a robust strategy to tune dielectric, piezoelectric, and transport properties in Bi-containing materials.

Conflicts of interest

There are no conflicts to declare.

Acknowledgements

T.F., A.A., and K.G.W. gratefully acknowledge financial support by the Deutsche Forschungsgemeinschaft under WE 4972/2

View Article Online
DOI: 10.1039/C7TC03975A

and FR 3718/1-1. T.F. thanks Dr. Edvinas Navickas for his help with the ToF-SIMS measurements. M.A. acknowledges the support of the Feodor Lynen Research Fellowship Program of the Alexander von Humboldt Foundation. M.D. and L.M.-L. acknowledge financial support from the Hessen State Ministry of Higher Education, Research and the Arts via LOEWE RESPONSE. L.M.-L. acknowledges financial support from DFG Grant MO 3010/3-1.

Notes and references

1. J. Rödel, W. Jo, K. T. P. Seifert, E.-M. Anton, T. Granzow and D. Damjanovic, *Journal of the American Ceramic Society*, 2009, **92**, 1153-1177.
2. W. Jo, R. Dittmer, M. Acosta, J. Zang, C. Groh, E. Sapper, K. Wang and J. Rödel, *Journal of Electroceramics*, 2012, **29**, 71-93.
3. J. Rödel, K. G. Webber, R. Dittmer, W. Jo, M. Kimura and D. Damjanovic, *Journal of the European Ceramic Society*, 2015, **35**, 1659-1681.
4. E. Taghaddos, M. Hejazi and A. Safari, *Journal of Advanced Dielectrics*, 2015, **05**, 1530002.
5. H. Zhang, C. Groh, Q. Zhang, W. Jo, K. G. Webber and J. Rödel, *Advanced Electronic Materials*, 2015, **1**, 1500018.
6. K. Reichmann, A. Feteira and M. Li, *Materials*, 2015, **8**, 5469.
7. R. R. McQuade and M. R. Dolgos, *Journal of Solid State Chemistry*, 2016, **242, Part 2**, 140-147.
8. M. Li, M. J. Pietrowski, R. A. De Souza, H. Zhang, I. M. Reaney, S. N. Cook, J. A. Kilner and D. C. Sinclair, *Nature Materials*, 2014, **13**, 31-35.
9. M. Li, H. Zhang, S. N. Cook, L. Li, J. A. Kilner, I. M. Reaney and D. C. Sinclair, *Chemistry of Materials*, 2015, **27**, 629-634.
10. L. Koch, S. Steiner, K.-C. Meyer, I.-T. Seo, K. Albe and T. Frömling, *Journal of Materials Chemistry C*, 2017, **5**, 8958-8965.
11. L. Li, M. Li, H. Zhang, I. M. Reaney and D. C. Sinclair, *Journal of Materials Chemistry C*, 2016, **4**, 5779-5786.
12. Y. A. Genenko, J. Glaum, M. J. Hoffmann and K. Albe, *Materials Science and Engineering: B (Advanced Functional Solid-State Materials)*, 2015, **192**, 52-82.
13. M. Acosta, L. A. Schmitt, L. Molina-Luna, M. C. Scherrer, M. Brilz, K. G. Webber, M. Deluca, H.-J. Kleebe, J. Rödel and W. Donner, *Journal of the American Ceramic Society*, 2015, **98**, 3405-3422.
14. J. Koruza, V. Rojas, L. Molina-Luna, U. Kunz, M. Duerrschnabel, H.-J. Kleebe and M. Acosta, *Journal of the European Ceramic Society*, 2016, **36**, 1009-1016.
15. M. Acosta, L. A. Schmitt, C. Cazorla, A. Studer, A. Zintler, J. Glaum, H.-J. Kleebe, W. Donner, M. Hoffman, J. Rödel and M. Hinterstein, *Scientific Reports*, 2016, **6**, 28742.
16. N. Liu, M. Acosta, S. Wang, B.-X. Xu, R. W. Stark and C. Dietz, *Scientific Reports*, 2016, **6**, 36910.
17. S.-E. Park and K. S. Hong, *Journal of Materials Research*, 1997, **12**, 2152-2157.
18. J. R. Gomah-Pettry, P. Marchet, A. Salak, V. M. Ferreira and J. P. Mercurio, *Integrated Ferroelectrics*, 2004, **61**, 159-162.
19. J. R. Gomah-Pettry, A. N. Salak, P. Marchet, V. M. Ferreira and J. P. Mercurio, *physica status solidi (b)*, 2004, **241**, 1949-1956.
20. J.-R. Gomah-Pettry, S. Said, P. Marchet and J.-P. Mercurio, *Journal of the European Ceramic Society*, 2004, **24**, 1165-1169.
21. S. T. Zhang, A. B. Kounga, E. Aulbach, H. Ehrenberg and J. Rodel, *Applied Physics Letters*, 2007, **91**, 3.
22. Y. Hiruma, Y. Imai, Y. Watanabe, H. Nagata and T. Takenaka, *Applied Physics Letters*, 2008, **92**, 262904.
23. D. Rout, K.-S. Moon, S.-J. L. Kang and I. W. Kim, *Journal of Applied Physics*, 2010, **108**, 084102.
24. K. Wang, A. Hussain, W. Jo and J. Rödel, *Journal of the American Ceramic Society*, 2012, **95**, 2241-2247.
25. F. Wang, M. Xu, Y. Tang, T. Wang, W. Shi and C. M. Leung, *Journal of the American Ceramic Society*, 2012, **95**, 1955-1959.
26. B. Parija, S. K. Rout, L. S. Cavalcante, A. Z. Simões, S. Panigrahi, E. Longo and N. C. Batista, *Appl Phys A*, 2012, **109**, 715-723.
27. F. Wang, C. M. Leung, Y. Tang, T. Wang and W. Shi, *Journal of Applied Physics*, 2013, **114**, 164105.
28. X. L. Zhao, W. Z. Yang, X. Q. Liu and X. M. Chen, *J Mater Sci: Mater Electron*, 2014, **25**, 1517-1526.
29. C. Tian, F. Wang, X. Ye, Y. Xie, T. Wang, Y. Tang, D. Sun and W. Shi, *Scripta Materialia*, 2014, **83**, 25-28.
30. A. Maqbool, A. Hussain, J. Ur Rahman, T. Kwon Song, W.-J. Kim, J. Lee and M.-H. Kim, *Ceramics International*, 2014, **40**, 11905-11914.
31. H.-L. Li, Q. Liu, J.-J. Zhou, K. Wang, J.-F. Li, H. Liu and J.-Z. Fang, *Journal of the European Ceramic Society*, 2016, **36**, 2849-2853.
32. X.-Y. Tong, H.-L. Li, J.-J. Zhou, H. Liu and J.-Z. Fang, *Ceramics International*, 2016, **42**, 16153–16159.
33. S. Kim, H. Choi, S. Han, J. S. Park, M. H. Lee, T. K. Song, M.-H. Kim, D. Do and W.-J. Kim, *Journal of the European Ceramic Society*, 2017, **37**, 1379-1386.
34. J.-K. Lee, K. S. Hong, C. K. Kim and S.-E. Park, *Journal of Applied Physics*, 2002, **91**, 4538-4542.
35. H. E. Mgbemere, R. P. Fernandes and G. A. Schneider, *Journal of the European Ceramic Society*, 2013, **33**, 3015-3022.
36. T. Frömling, J. Hou, W. Preis, W. Sitte, H. Hutter and J. Fleig, *Journal of Applied Physics*, 2011, **110**, 043531.
37. T. Frömling, A. Schintlmeister, H. Hutter and J. Fleig, *Journal of the American Ceramic Society*, 2011, **94**, 1173-1181.
38. T. Frömling, H. Hutter and J. Fleig, *Journal of the American Ceramic Society*, 2012, **95**, 1692-1700.
39. G. Holzlechner, M. Kubicek, H. Hutter and J. Fleig, *Journal of Analytical Atomic Spectrometry*, 2013, **28**, 1080-1089.
40. J. Maier, in *Physical Chemistry of Ionic Materials*, John Wiley & Sons, Ltd, 2005, DOI: 10.1002/0470020229.ch6, pp. 268-398.
41. R. T. P. Whipple, *The London, Edinburgh, and Dublin Philosophical Magazine and Journal of Science*, 1954, **45**, 1225-1236.
42. A. D. Le Claire, *British Journal of Applied Physics*, 1963, **14**, 351.
43. H. Mehrer, *Diffusion in solids*, Springer-Verlag Berlin Heidelberg, Berlin, Germany, 2007.

View Article Online
DOI: 10.1039/C7TC03975A

44. S. Koerfer, R. A. De Souza, H.-I. Yoo and M. Martin, *Solid State Sciences*, 2008, **10**, 725-734.
45. M. Izuki, M. E. Brito, K. Yamaji, H. Kishimoto, D.-H. Cho, T. Shimonosono, T. Horita and H. Yokokawa, *Journal of Power Sources*, 2011, **196**, 7232-7236.
46. I.-T. Seo, S. Steiner and T. Frömling, *Journal of the European Ceramic Society*, 2017, **37**, 1429-1436.
47. Y.-I. Jung, S.-Y. Choi and S.-J. L. Kang, *Acta Materialia*, 2006, **54**, 2849-2855.
48. S.-M. An and S.-J. L. Kang, *Acta Materialia*, 2011, **59**, 1964-1973.
49. A. A. Bokov and Z. G. Ye, *Journal of Materials Science*, 2006, **41**, 31-52.
50. S.-T. Zhang, A. B. Kounga, E. Aulbach, H. Ehrenberg and J. Rödel, *Applied Physics Letters*, 2007, **91**, 112906.
51. W. Jo, T. Granzow, E. Aulbach, J. Rödel and D. Damjanovic, *Journal of Applied Physics*, 2009, **105**, 094102.
52. R. Dittmer, K. G. Webber, E. Aulbach, W. Jo, X. Tan and J. Roedel, *Acta Materialia*, 2013, **61**, 1350-1358.
53. S. Huband and P. A. Thomas, *Journal of Applied Physics*, 2017, **121**, 184105.
54. N. Setter, *Ferroelectrics*, 2016, **500**, 164-182.
55. H. S. Shulman, D. Damjanovic and N. Setter, *Journal of the American Ceramic Society*, 2000, **83**, 528-532.
56. A. Mahajan, H. Zhang, J. Wu, E. V. Ramana, M. J. Reece and H. Yan, *The Journal of Physical Chemistry C*, 2017, **121**, 5709-5718.
57. W. Jo, S. Schaab, E. Sapper, L. A. Schmitt, H.-J. Kleebe, A. J. Bell and J. Rödel, *Journal of Applied Physics*, 2011, **110**, 074106.
58. J. Zang, M. Li, D. C. Sinclair, W. Jo and J. Rödel, *Journal of the American Ceramic Society*, 2014, **97**, 1523-1529.
59. J. Zang, M. Li, D. C. Sinclair, T. Frömling, W. Jo and J. Rödel, *Journal of the American Ceramic Society*, 2014, **97**, 2825-2831.
60. J. Glaum, M. Zakhozheva, M. Acosta, E. Aksel, H.-J. Kleebe, M. Hoffman and L. A. Schmitt, *Journal of the American Ceramic Society*, 2016, **99**, 2801-2808.
61. P.-Y. Chen, C.-S. Chen, C.-S. Tu and T.-L. Chang, *Journal of the European Ceramic Society*, 2014, **34**, 4223-4233.

View Article Online
DOI: 10.1039/C7TC03975A

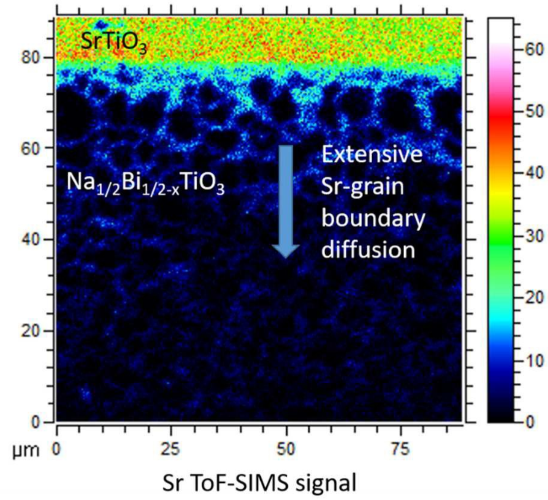

Designing Properties of $(Na_{1/2}Bi_x)TiO_3$-Based Materials Through A-Site Non-Stoichiometry

Till Frömling, Sebastian Steiner, Azatuhi Ayrikyan, Daniel Bremecker, Michael Dürrschnabel, Leopoldo Molina-Luna, Hans-Joachim Kleebe, Herbert Hutter, Kyle Webber, Matias Acosta

Modification of microstructure and electrical properties due to high A-site diffusion of cations induced by non-stoichiometry during processing